

Soft X-ray refractive index by reconciling total electron yield with specular reflection: experimental determination of the optical constants of graphite

C. Jansing,^a H. Wahab,^b H. Timmers,^b A. Gaupp^c and H.-C. Mertins^{a*}

Received 15 May 2018

Accepted 18 July 2018

Edited by V. Favre-Nicolin, CEA and Université Joseph Fourier, France

Keywords: soft X-rays; optical constants; X-ray spectroscopy; graphite; birefringence.

Supporting information: this article has supporting information at journals.iucr.org/s

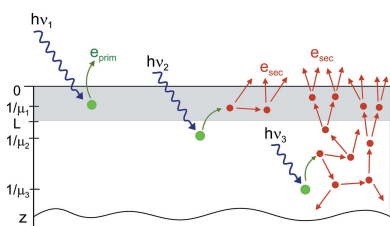
^aUniversity of Applied Sciences Münster, Stegerwaldstrasse 39, D-48565 Steinfurt, Germany, ^bThe University of New South Wales, UNSW Canberra, ACT 2600, Australia, and ^cHZB, Albert-Einstein-Strasse 15, D-12489 Berlin, Germany. *Correspondence e-mail: mertins@fh-muenster.de

The complex refractive index of many materials is poorly known in the soft X-ray range across absorption edges. This is due to saturation effects that occur there in total-electron-yield and fluorescence-yield spectroscopy and that are strongest at resonance energies. Aiming to obtain reliable optical constants, a procedure that reconciles electron-yield measurements and reflection spectroscopy by correcting these saturation effects is presented. The procedure takes into account the energy- and polarization-dependence of the photon penetration depth as well as the creation efficiency for secondary electrons and their escape length. From corrected electron-yield spectra the absorption constants and the imaginary parts of the refractive index of the material are determined. The real parts of the index are subsequently obtained through a Kramers–Kronig transformation. These preliminary optical constants are refined by simulating reflection spectra and adapting them, so that measured reflection spectra are reproduced best. The efficacy of the new procedure is demonstrated for graphite. The optical constants that have been determined for linearly polarized synchrotron light incident with *p*- and *s*-geometry provide a detailed and reliable representation of the complex refractive index of the material near π - and σ -resonances. They are also suitable for allotropes of graphite such as graphene.

1. Introduction

Soft X-ray spectroscopies with polarized synchrotron radiation are effective characterization techniques that are successfully applied in a number of fields such as the physical and biological sciences as well as in materials engineering (Stöhr, 1996; Stöhr & Siegmann, 2006). It may be surprising that the soft X-ray optical constants of many materials are not well known at energies spanning resonances associated with absorption edges. It has been demonstrated by us in previous work (Mertins *et al.*, 2004; Wahab *et al.*, 2018) that information about a sample from absorption and reflection spectra can contain independent and complementary information. This can also be exploited in the determination of optical constants.

Due to the importance of organic chemistry in many applications, the study of carbonaceous samples is of particular interest to X-ray spectroscopists. In this case the resonances near the carbon 1s edge cause saturation effects in total-electron-yield (TEY) spectra that distort the optical constants extracted from such data if those effects are not corrected. The lack of reliable optical constants for graphitic materials near the carbon 1s edge is particularly felt since the advent of graphene research (Novoselov *et al.*, 2012). The



© 2018 International Union of Crystallography

resonant excitation of carbon 1s core electrons to anti-bonding orbitals enables the identification of the electronic structure of carbon in organic molecules as well as in graphitic material systems. This includes thin film systems that contain two-dimensional graphene layers. Moreover, the bonding characteristics and spatial orientation of organic groups that are adventitiously or deliberately adsorbed at graphite and graphene surfaces may be determined (Stöhr, 1996; Wahab *et al.*, 2018). The deliberate adsorption of such molecules is an important aspect of the tailoring of graphene materials to biomedical applications (Jiang, 2011; Shen *et al.*, 2012). In the case of solids, soft X-ray spectroscopies can furthermore provide information on the electronic band structure of a material, since the spectra reflect the density of electronic states (Stöhr, 1996; Stöhr & Siegmann, 2006). The probing depths of different types of spectroscopies differ, so that volume-sensitive and surface-sensitive investigations of a material are both possible.

Absorption spectroscopy of soft X-ray photons can be performed with several methods. A direct determination of the absorption cross-section is possible for thin samples that permit transmission measurements of soft X-ray light. A number of indirect methods exist for the study of bulk samples. Those include TEY, partial electron yield, fluorescence, photoelectron and Auger-electron spectroscopy. With these indirect methods the observed spectra need to be manipulated to yield the X-ray photon absorption spectrum by using suitable theoretical assumptions (Stöhr, 1996; Stöhr & Siegmann, 2006). The reproduction of results in simulations would benefit from accurate optical constants.

The reflection of incident soft X-ray photons permits typically a deeper probing depth than achievable with absorption methods, since the detected particle is a soft X-ray photon at relatively high energy. In contrast to absorption spectroscopy, where these parameters are not available, the polarization and the phase of the reflected light carry independent information about the interaction with the material. On reflection the polarization of the light is typically changed. This change can, for example, provide information on the electromagnetic fields in a sample. Furthermore, the interference of light reflected at different dielectric boundaries of a multilayer system depends sensitively on the thickness of the layers. Such thicknesses can thus be accurately determined from reflection spectra.

In order to interpret measured reflection spectra and permit the theoretical modelling of the physical properties of samples, a detailed knowledge of the complex refractive index of a material, *i.e.* of its optical constants, is indispensable. The optical constants determine both the refraction and the absorption of soft X-rays in this material. In order to determine a complete set of optical constants, typically the absorption cross-section is interpreted as the imaginary part of the complex refractive index. The absorption cross-section is typically obtained *via* electron-yield measurements. The real part of the constants that relates to refraction is then deduced by performing a Kramers–Kronig transformation of the measured absorption data (Stöhr, 1996). This procedure,

however, is not straightforward, since the probing depth depends on the angle of incidence and results for the same sample may differ accordingly. Furthermore, the relationship between a measured electron yield and the corresponding photon absorption cross-section is not necessarily linear. In particular, in the interesting resonance region near absorption edges, where optical constants vary dramatically with energy, saturation effects in the measured yield are known to be problematic (Henneken *et al.*, 1999, 2000; Nakajima *et al.*, 1999). An indirect determination of absorption *via* electron-yield measurements alone can thus not necessarily be expected to give the correct set of optical constants that would correctly apply in the reflection of soft X-ray light.

A correct quantification of the soft X-ray photon absorption cross-section can be achieved through the direct determination of the energy-dependent absorption constant μ in transmission experiments using thin samples. In this case incident light of intensity I_0 is transmitted through a sample of known thickness x and the resultant intensity $I = I_0 \exp(-\mu x)$ can be measured behind the sample. However, in the soft X-ray range the photon absorption cross-section is so large that extremely thin self-supporting films are required for such direct measurements. In the case of carbon at energies spanning the 1s absorption edge a thickness of less than 100 nm is necessary. Moreover, reducing the thickness further limits experimental accuracy, since the film thickness has to be well known.

A much more straightforward alternative is the detection of the TEY of bulk samples of conducting material (Gudat & Kunz, 1972; Henke *et al.*, 1981). In this case the TEY can be reliably determined by measuring the drain current of the sample when light is incident. Alternatively, the fluorescence yield (FLY) may be measured (Stöhr, 1996). Generally both the measured TEY and the measured FLY are linearly proportional to the product of absorption constant μ and photon energy $h\nu$. It is, however, well known that this proportionality does not hold at energies spanning resonant core level excitations where photon absorption is particularly strong. Saturation occurs in both the TEY and the FLY, so that both measured yields do not correctly represent true absorption peaks. Consequently, locally the insufficient height of the observed peak does not yield the constant μ correctly and, if this height is taken literally, the optical constants deduced for those energies are also incorrect (Nakajima *et al.*, 1999).

Before discussing the origin of saturation effects in TEY and FLY spectra in detail, we list a number of important conditions that are required so that a linear proportionality between TEY and FLY on one hand and the product of absorption constant and photon energy on the other may be assumed in good approximation (Henke *et al.*, 1981; Stöhr, 1996). These conditions for linear proportionality are:

- (1) The primary electron yield may be neglected relative to the yield of secondary electrons.
- (2) The sample thickness is large compared with the electron escape length L .
- (3) The sample thickness is large compared with the photon penetration depth $1/\mu$.

(4) The penetration depth $1/\mu$ is large compared with the electron escape length L .

(5) Photon reflection and, in the case of TEY measurements, fluorescence may be neglected.

If these five conditions are not fulfilled, saturation effects occur that affect the yield measurements. This becomes significant at resonance energies.

Nakajima *et al.* (1999) discuss these limits in the applicability of TEY spectroscopy towards the determination of optical constants, but they do not suggest a correction procedure. Suggestions to overcome the saturation effects in order to obtain correct absorption spectra have, however, been made by other authors.

Achkar *et al.* (2011) have, for example, established the technique of an inverse partial fluorescence yield spectroscopy, which is applicable to polyatomic materials. In that technique the absorption constant μ_A of atom A is deduced from the detection of the fluorescence intensity I_B of atom B . The intensity I_B is proportional to the number of photons that cause excitations which itself is proportional to the penetration depth $1/\mu_A$ of the incident photons. Atoms of type A thus work like a filter for atoms of type B . This clever technique is, however, quite complex since it requires that the fluorescence yield is analysed with a monochromator. Importantly, the technique is not applicable to monoatomic materials such as graphite.

Filatova & Sokolov (2018) have suggested that total external reflection spectroscopy may be used to deduce the optical constants. In their approach the measured reflection spectra are Kramers–Kronig-transformed to give the absorption coefficients. This requires, however, that all five conditions listed above are met. Moreover, due to the required small grazing angle of incidence of $2\text{--}3^\circ$, this technique is extremely surface-sensitive and it requires the *in situ* preparation and the precise positioning of samples inside the vacuum chamber.

In this paper we present an alternative procedure that reconciles measured TEYs with simultaneously measured spectra of specular reflection. Our new procedure can provide a reliable set of optical constants across resonance regions. In particular, this approach corrects the saturation effects in the TEY spectra that obscure the correct absorption cross-section. We have demonstrated the procedure for highly oriented pyrolytic graphite (HOPG) for two different linear polarizations of the incident soft X-ray light. Moreover, we have determined a detailed set of optical constants at energies spanning the carbon $1s$ absorption edge.

In our approach the saturation effects in TEY spectra are corrected using a self-consistent procedure. Specifically, the efficiency of the creation of secondary electrons by an incident soft X-ray photon, M , is modelled using an energy-dependent function that is extracted from a TEY measurement for the sample. This energy-dependent efficiency then permits a meaningful correction of the measured TEY spectrum. The corrected TEY spectrum represents the absorption constant μ well at all energies and can be renormalized to give the imaginary part of the complex refractive index. The corre-

sponding real part of the index can be derived conventionally via a Kramers–Kronig transformation, so that a preliminary set of optical constants is obtained. The preliminary set of optical constants is then applied in calculations of reflection spectra for the same sample using the Fresnel equations. Iteratively by scaling the efficiency of secondary electron creation, the calculated reflection spectra are adapted to measured reflection spectra that have been recorded simultaneously with the TEY measurement. From the best adaptation of the simulation to the reflection data, a refined set of optical constants is finally obtained.

2. Self-consistent procedure for the determination of soft X-ray optical constants

Fig. 1 illustrates important interactions in a material that follow the absorption of a soft X-ray photon. The sketch emphasizes the depth-dependence of the yield of escaping electrons.

2.1. Total observable electron yield

The X-ray absorption cross-section is conventionally taken to be proportional to the number of core holes that are created by the photons impinging the material (Stöhr, 1996; Stöhr & Siegmann, 2006). The excited core electron can be ejected directly or it can form an exciton in the material, *i.e.* a mobile electron–hole pair. The filling of a core hole leads predominantly to the emission of Auger electrons, a process that is, for light materials such as graphite, about a factor of 100 stronger than the alternative fluorescence decay. Due to scattering processes primary electrons tend to create a cascade of low-energy secondary electrons (Fig. 1). When the initial interaction occurs at a depth z less than the typical escape length L , secondary electrons can leave the sample surface and can be detected in measurements of the electron yield.

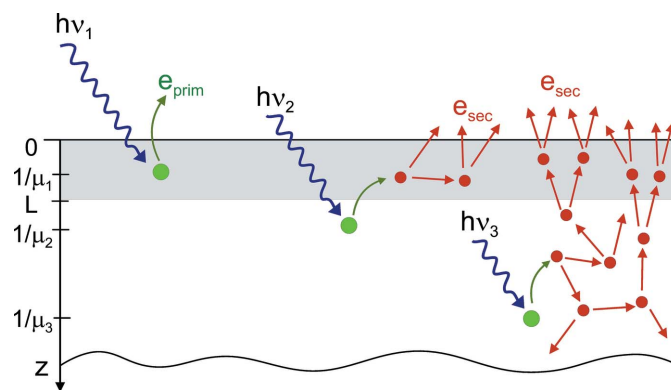


Figure 1 Sketch of typical interaction processes that occur as a consequence of the absorption of a photon with energy $h\nu$. A primary electron e_{prim} may be ejected (left) or alternatively an avalanche of secondary electrons e_{sec} can be created by electron scattering (right). The relative importance of these two processes depends on the material depth z . With decreasing absorption constant $\mu_1 > \mu_2 > \mu_3$ the penetration depth $1/\mu$ of the photon increases and the ratio of escaping secondary to primary electrons increases too. The electron escape length L is indicated schematically for reference.

The number of secondary electrons per incident photon is often taken to be proportional to the product of the energy $h\nu$ of the incident photon and a material constant M that expresses the efficiency of converting this energy into secondary electrons (Stöhr, 1996). The inverse $\varepsilon = 1/M$ represents therefore a mean energy that is necessary for the creation of a single secondary electron that is able to escape the sample and thus will contribute to the electron yield spectrum. Assuming that M is constant and independent of the energy of the incident X-ray photon, as well as neglecting primary electrons in good assumption [see Condition (1) above], means that TEY η and absorption constant μ are linearly proportional.

One may consider now the number of electrons dN_z created within the interval dz at the depth z in a macroscopically thick sample. The electron yield per incident photon at depth z is then $d\eta_z = dN_z/I_0$ and the absorption law can be written as (Stöhr, 1996; Nakajima *et al.*, 1999; Sohn *et al.*, 2009)

$$d\eta_z = \frac{\mu}{\cos\theta} \exp(-\mu z / \cos\theta) dz, \quad (1)$$

where $x = z/\cos\theta$ is the path length of the incident photon inside the material and θ is the angle of incidence with respect to the surface normal.

The escape probability for the secondary electrons decreases exponentially with distance from the sample surface. Consequently the number of secondary electrons per absorbed incident photon that escape and contribute to the TEY is given by

$$d\eta_z = h\nu M \exp(-\mu z / \cos\theta) \frac{\mu}{\cos\theta} \exp(-z/L)(1 - R) dz. \quad (2)$$

Here L is the escape length of electrons. The efficiency of creating secondary electrons per incident photon is represented by the term $h\nu M$ (Stöhr, 1996). The reflectance of the material surface is equal to R . In the soft X-ray range the reflectance can generally be neglected for large grazing incidence angles, since then $R \simeq 0$. This approximation typically holds well at incidence angles $\theta > 80^\circ$ and is also expressed by Condition (5) above that will be assumed in this consideration. Integration over the sample thickness, which is large compared with the photon penetration depth [see Condition (3)], gives the TEY (Henneken *et al.*, 2000) as

$$\eta = \frac{1}{2} M\mu L \frac{1}{\cos\theta} h\nu \frac{1}{1 + \mu L / \cos\theta}. \quad (3a)$$

This equation can be simplified if the TEY η is assumed to be linearly proportional to the product of absorption constant μ and photon energy $h\nu$. It reads then

$$\eta = \frac{1}{2} M\mu L h\nu / \cos\theta. \quad (3b)$$

Equation (3a) clearly shows that a proportionality of the product $\mu \cdot h\nu$ and the TEY η is given only for the case that M and L are both independent of photon energy. Secondly, the proportionality holds only true if $\mu L / \cos\theta \simeq 0$. This is the mathematical expression of Condition (4).

Any dependence of M on photon energy $h\nu$ can cause deviations from proportionality. This occurs in particular at energies where the resonant absorption of photons dominates. In order to achieve an effective correction, the energy dependence of $M = 1/\varepsilon$ and the role of the term $1/(1 + \mu L / \cos\theta)$ are therefore explicitly to be considered in the next section.

It may be noted for completeness that, in the case of thin samples of thickness d , Conditions (2) and (3) are not fulfilled and that the TEY η is given by the more complicated expression

$$\eta = \frac{1}{2} M\mu L \frac{1}{\cos\theta} h\nu \frac{1}{1 + \mu L / \cos\theta} \times \left\{ 1 - \exp \left[-d \left(\frac{1}{L} + \frac{\mu}{\cos\theta} \right) \right] \right\}. \quad (4)$$

This equation is equivalent to equation (3a) which holds for thick samples where d is large compared with the electron escape depth L and also large with respect to the penetration depth of light ($d \gg 1/\mu$).

2.2. Optical constants

Since the complex refractive index relates to both the refraction and the absorption of light, a simultaneous measurement of reflection and absorption can provide a reliable complete set of optical constants, if the absorption spectrum is accurately established by correcting the saturation effects in electron-yield data.

2.2.1. Absorption spectrum. Knowledge of the complex refractive index $\tilde{n} = n + ik$ of a material permits a full description of the transmission, reflection and absorption of soft X-ray light through the application of these optical constants in the Fresnel equations (Born & Wolf, 1959). In the soft X-ray range the real part of the index, $n = 1 - \delta$, is close to unity and the imaginary part, k , is related to the absorption constant *via* $\mu = 4\pi k/\lambda$, where the photon wavelength is indicated by λ . The values of n and k depend both on the photon energy and also on the polarization of the incident light. These two optical constants are also related to the scattering factors f_1 and f_2 according to

$$f_1 = \frac{2\pi}{r_0\lambda^2 N} \delta, \quad (5a)$$

$$f_2 = \frac{2\pi}{r_0\lambda^2 N} k, \quad k = \mu \lambda / 4\pi. \quad (5b)$$

Here the atomic number density is denoted by N and the Lorentz radius of the electrons is represented by r_0 .

An independent measurement of the scattering factors f_1 and f_2 is possible only by ellipsometry, which is technically challenging in the soft X-ray range (Azzam & Bashara, 1987; Schäfers *et al.*, 1999). A feasible alternative is, however, the use of TEY spectroscopy in combination with reflectometry, which is the approach that is successfully demonstrated in this paper. From the electron-yield data the energy-dependence of the absorption constant can be obtained. Using equation (5b)

the scattering factor f_2 can then be deduced. The corresponding scattering factor f_1 can subsequently be obtained from f_2 via a Kramers–Kronig transformation. This is achieved by calculating the principal value integral as given by (Born & Wolf, 1959)

$$f_1(E) = Z^* - \frac{2}{\pi} P \int_0^{\infty} \frac{E_2 f_2(E_2)}{E_2^2 - E^2} dE_2, \quad (6)$$

with the relativistic correction Z^* . The validity of the scattering factors can then be established independently by testing them against reflection spectra measured for the same sample. The integration in equation (6) over the energy E_2 extends from zero to infinity. Several computer codes exist that can determine this integral, e.g. the code developed by Watts (2014) that was used in this work.

Since the optical constants vary considerably at energies near absorption edges where strong resonance effects occur, the focus of this work is on such resonance regions. Outside these resonance regions the optical constants are already well known and tabulated, e.g. in the tables by Henke *et al.* (1993). In order to calculate the integral in equation (6) the range of experimental determined data for $f_2(E_2)$ is typically extrapolated towards zero and towards infinity, respectively, using the established tables by Henke and co-workers. This was also done here.

The crucial step in the determination of the optical constants is thus the initial extraction of absorption constants μ from experimental TEYs η . As we have elaborated in §2.1 above, the saturation of the observed electron yield near resonance peaks is of particular concern. We have trialled four different ways to address this well known problem. In each approach the absorption constant μ is determined in a somewhat different way. The associated four equations are listed below:

$$\mu = \eta \frac{2\varepsilon \cos \theta}{L h\nu}, \quad \varepsilon = \text{constant}, \quad (7a)$$

$$\mu = \eta \frac{2\varepsilon \cos \theta}{L h\nu}, \quad \varepsilon(h\nu), \quad (7b)$$

$$\mu = \eta \frac{\cos \theta}{(h\nu/2\varepsilon - \eta)L}, \quad \varepsilon = \text{constant}, \quad (7c)$$

$$\mu = \eta \frac{\cos \theta}{(h\nu/2\varepsilon - \eta)L}, \quad \varepsilon(h\nu). \quad (7d)$$

Equation (7a) is a straight rearrangement of equation (3b). It thus holds only true if $\mu L/\cos \theta \simeq 0$. This is the conventional approach, which assumes proportionality between TEY η and the absorption constant μ . Equation (7b) takes into account an energy-dependence of the mean energy $\varepsilon = 1/M$ that is required to create a secondary electron. Equation (7c) is a rearrangement of equation (3a) with $\mu L/\cos \theta \neq 0$. Finally, equation (7d) is the same as equation (7c); however, it considers in addition a dependence of ε on photon energy $h\nu$.

For the evaluation of all four equations (7a)–(7d) the electron escape length L needs to be known. The parameter can be deduced from photo-electron experiments. For HOPG, which is the material of interest in this work, Sohn *et al.* (2009) found $L = 1.95$ nm and, for comparison, for the metals Au and Cu, Henneken *et al.* (2000) determined $L = 1.9$ nm. The latter authors have also published values for M for the same two metals of 0.0156 eV^{-1} and 0.0380 eV^{-1} , which corresponds to mean energies of $\varepsilon = 64 \text{ eV}$ and $\varepsilon = 26 \text{ eV}$, respectively (Henneken *et al.*, 1999, 2000). Following the work by Sohn *et al.* (2009) we apply in this work for HOPG the value $L = 1.95$ nm. The efficiency of secondary electron creation $\varepsilon = 1/M$ has been obtained, however, using the iterative procedure that is described below.

2.2.2. Reflection spectrum. The specular reflection of a photon is the consequence of the virtual excitation and de-excitation of a core electron. The reflection spectrum can be simulated using the Fresnel equations, once a complete set of optical constants is known (Born & Wolf, 1959). As described in §2.2.1 above, initially a preliminary set of optical constants was extracted from measured TEY spectra assuming the direct proportionality between TEY and absorption constant μ as it is expressed by equation (7a).

With these preliminary optical constants reflection spectra were simulated for the experimental conditions used in this work. Differences between the simulation and the reflection data, which were recorded along with the TEY measurement, were then reduced iteratively by adaptation. In this adaptation of the simulation, equations (7b) and (7c) were considered and the mean creation energy ε was chosen to achieve the best agreement. In particular, an energy dependence was considered. The optical constants that resulted in the best agreement between simulated and measured reflection data have been adopted as a detailed set.

The strength of our new procedure therefore results from the reconciliation of two independent experimental measurements, namely the simultaneous determination of the TEY and of the reflectance. Moreover, apart from a reliable determination of the complex refractive index, the procedure determines also the energy dependence of the mean energy that is required to create a secondary electron in a material.

3. Experimental setup

The room-temperature experiments were performed on the Apple-type undulator beamline UE56-2-PGM2 of BESSY (Weiss *et al.*, 2001). The spectral resolution near 280 eV was $E/\Delta E = 2000$ and the accuracy of the absolute energy calibration was better than 0.1 eV.

The samples were HOPG of mosaicity 0.4° . Before introduction into the vacuum of the measurement chamber, which was 2×10^{-9} mbar, a sliver of material was cleaved from the sample to achieve a pristine surface. The glancing angle of the light beam with the sample surface was always 20.4° . Rotation of the sample about the beam axis permitted changes of the scattering plane. During the measurements the relative orientation of scattering plane and sample was such that the

electric field vector of the incoming linearly polarized light was either in the scattering plane (p -geometry) or normal to it (s -geometry), respectively. The degree of linear polarization was $P_L > 0.99$, which was established following a method described by Schäfers *et al.* (1999).

The TEY generated by the incident light beam was measured by recording the drain current from the HOPG sample using a Keithley picoammeter (Model 6482). The intensity of the specular reflex from the sample at a reflection angle with respect to the surface of 20.4° was measured simultaneously with a Hamamatsu GaAs:P diode (Krumrey *et al.*, 1988). Since the HOPG sample and the diode could be moved *in situ* under vacuum using external controls, the incident and reflected light could be measured with the same diode. This allowed the determination of absolute specular reflectances. Further details about the measurement setup and the normalization procedures that were used have been published previously (Jansing *et al.*, 2016).

4. Results

The TEY η measured with p -geometry and with s -geometry, respectively, are shown in Fig. 2. The two scattering geometries correspond to the two different relative orientations of polarization direction and surface normal. For p -geometry and for small glancing angles, the polarization direction almost aligns with the surface normal. In the case of s -geometry, in contrast, polarization direction and surface normal are orthogonal.

In the measured TEY spectra the strong exciton resonances at 285.1 eV (π -resonance) and at 291.5 eV (σ -resonance), respectively, clearly show up, accompanied at higher energies by an edge-like onset of transitions into the conduction band. Since the HOPG was cleaved just before introduction to vacuum, only a negligible signal due to adventitious adsor-

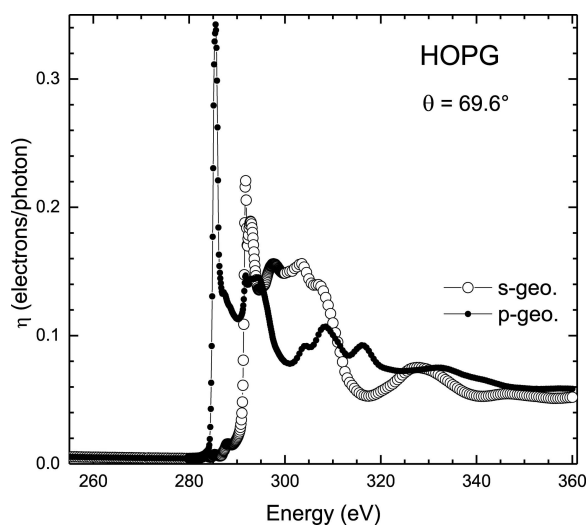


Figure 2
The TEY η measured across the carbon $1s$ absorption edge for a HOPG sample. Results have been obtained with linearly polarized X-ray light for p - (filled symbols) and s -geometry (open symbols), respectively. The angle of incidence was $\theta = 69.6^\circ$.

bates is observed with s -geometry near 288 eV. This demonstrates the pristine quality of the HOPG surface.

4.1. Constant conversion efficiency M

Fig. 3 shows the measured TEY spectrum for p -geometry in more detail as black open symbols with the yield η denoted on the left axis of ordinates. The data have been manipulated using equation (7c) and increasing values for the mean energy of secondary electron creation, ε , to give estimates of the absorption coefficient. The manipulated data are shown in colour as filled symbols and the absorption coefficient μ is plotted against the right-hand axis of ordinates.

A small value for ε , such as 1 eV, corresponds to a negligible number of primary electrons in the observed electron yield. This is the situation characterized by Condition (1). In this case the electron yield η can be neglected in the denominator of the right-hand side of equation (7c), since $h\nu/2\varepsilon$ is large. The assumption of direct proportionality between η and absorption constant μ is then appropriate and μ is given by equation (7a). It is apparent from Fig. 3 that for large values of ε the absorption coefficient is enhanced at the resonance at 285.1 eV. This is emphasized in the inset of the figure, which shows the resonance peak on a larger energy scale. With increasing values for ε the absorption constant μ also becomes

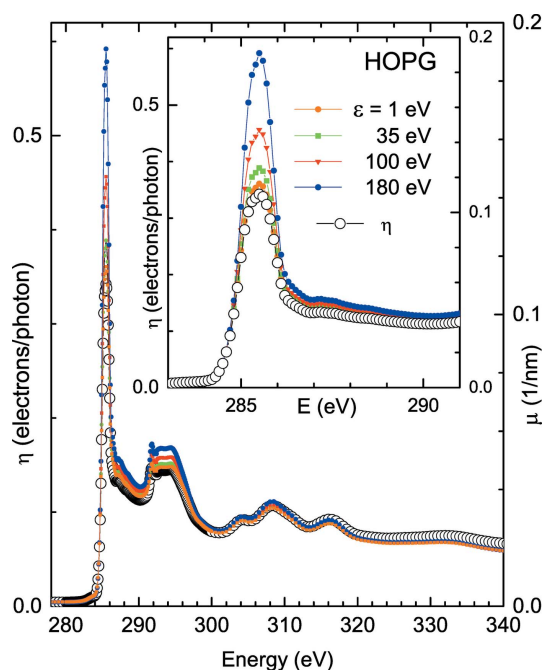


Figure 3
Determination of the absorption constants μ for HOPG for linearly polarized light incident with p -geometry. Using the procedure described in the text, manipulated TEY spectrum η (left axis of ordinates) is interpreted as the energy function of the absorption constant μ (right axis of ordinates). Open circles show the measured η . Filled symbols correspond to different constant values of the creation efficiency $M = 1/\varepsilon$. The inset shows in more detail the π -resonance peak, where differences are most pronounced. It is apparent that if the mean creation energy ε is increased, the problematic saturation of the measured yield at the resonance peak is appropriately compensated. An increase of ε corresponds to a reduction of the ratio of secondary to primary electrons.

larger at higher energies (290–320 eV). Below the resonance and far beyond there is insignificant change.

It may be noted that even a constant ε yields an absorption constant μ that is energy-dependent. This is because the TEY is a complicated function of photon energy, see Fig. 4 (top). In particular, at resonances, where a saturation of the observed electron yield occurs, the absorption is locally very large, which may be expected. The differences between equations (7a) and (7c) and associated effects in the energy-dependence of the absorption constant can be visualized well by considering the function

$$f = 1/(hv/2\varepsilon - \eta), \quad (8)$$

that takes in equation (7c) the place of $hv/2\varepsilon$ in equation (7a). This function may be denoted as the ‘correction function’ $f(hv, \varepsilon)$. It is plotted in Fig. 4 (bottom) on a logarithmic scale for the same values of ε that are shown in Fig. 3. The effect of the correction function f is a strong enhancement of the TEY data at resonances, *i.e.* achieving at those energies larger values of the absorption constant μ , and a more modest boost of the TEY data at energies outside resonances. The energy-dependence of the correction function is predominantly caused by the energy-dependence of η and the form of the denominator on the right-hand side of equation (8). In contrast the influence on the absorption constant by the term

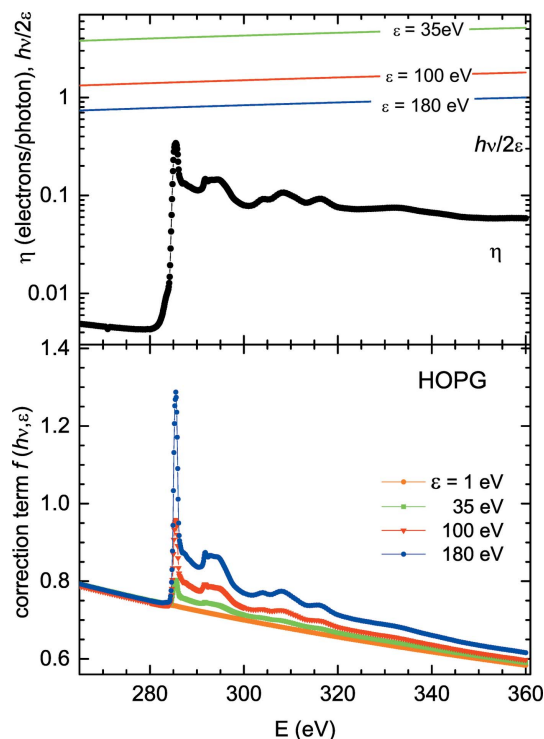


Figure 4

At the top a comparison on a logarithmic scale of the measured TEY spectrum η (filled circles) and the term $h\nu/2\varepsilon$ (lines) for different values of ε . With increasing mean energy ε the two terms become more and more of similar magnitude. At the bottom the correction term $f = 1/(h\nu/2\varepsilon - \eta)$ in equation (7c) is shown as a function of photon energy $E = h\nu$. It may be noted that in spite of a constant ε the correction term is energy-dependent and that the correction is most pronounced in the resonance region.

$h\nu/2\varepsilon$ in equation (7a), which is linear with photon energy $h\nu$, is relatively insignificant for constant values of ε .

In order to determine detailed and reliable optical constants from TEY measurements, two challenges must be addressed. Firstly, an appropriate relationship between TEY and absorption constant μ needs to be established. Secondly, the value and possible energy-dependence of the mean energy ε of creating secondary electrons that escape the material have to be decided.

In this work we have adopted the new approach to validate optical constants determined *via* TEY measurements using experimental reflection data that were simultaneously measured for the same sample. Using this self-consistent method the mean energy ε can be determined. Specifically by assuming a constant mean creation energy of $\varepsilon = 1$ eV a preliminary set of optical constants was obtained for HOPG using equation (7c). This set of constants was applied in simulations based on the Fresnel equations and performed with the code *KKcalc* by Watts (2014). In all such simulations the surface roughness of HOPG was set to $\zeta = 0.7$ nm (for details see §4.4). The mean creation energy ε was then treated as a free parameter. By comparing with the measured reflection spectra, the simulations were adapted to the reflectance data. This was achieved by selecting different constant values of ε and furthermore considering a possible energy-dependence. The efficacy of this adaptation is demonstrated in Fig. 5 for linearly polarized light incident with *p*-geometry. It is clear that, by assuming direct proportionality between yield and absorption [equation (7a)], no agreement between reflection experiment (open circles) and simulation (green curve) can be obtained. The simulated peak at the π -resonance is strongly

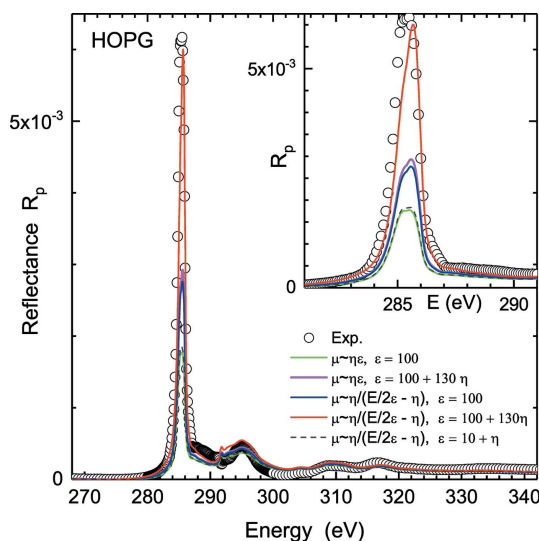


Figure 5

The reflectance R_p for HOPG measured with *p*-geometry and simulations. The experimental data (open circles) are best produced by a simulation that is based on optical constants that have been determined using an energy-dependent ε and equation (7d) (red curve). Other simulations are shown for comparison and discussed in the text. The inset compares the data and simulations in more detail at the π -resonance peak. (The values for ε are given in eV and the respective functional dependence of μ on η is indicated.)

underestimated due to the saturation of the electron yield observed at this resonance energy.

A somewhat better agreement between reflectometry experiment and simulation is obtained if the yield spectrum is corrected using equation (7c), although the resonance peak is generally underpredicted. The increase in the simulated reflectance is a consequence of larger optical constants due to the absorption enhancement of the absorption constant μ by the correction function $f(h\nu, \varepsilon)$. The choice of $\varepsilon = 100$ eV was found to give an absorption spectrum that produces a set of optical constants which achieve the best consistency in this case (Fig. 5, blue).

Increasing the constant value of ε further (e.g. $\varepsilon = 250$ eV) has been found to increase the peak height. In that case the resonance peak shifts, however, unreasonably by 0.4 eV to higher energies. A detailed exploration of such effects that are caused by varying the constant mean energy of secondary electron creation ε in equation (7c) has shown that further improvement of the agreement between the simulated and the measured reflection spectrum is not possible, unless the constancy of ε is relaxed. Thus an explicit energy-dependence of $M = 1/\varepsilon$ has been considered.

4.2. Energy-dependent conversion efficiency M

A dependence of $M = 1/\varepsilon$ on photon energy $h\nu$ may originate from the energy-dependent photon absorption depth. Accepting this, the efficiency of creating secondary electrons via scattering processes also has to be taken as depth-dependent.

In line with theory the absorption depth of incident photons may be associated with the penetration depth of the light, which is $1/\mu$ (Stöhr, 1996; Stöhr & Siegmann, 2006). Therefore, for small absorption constants μ , photons penetrate deep into the sample. Generally the fast primary electrons have to travel a relatively long path before they may reach the surface. Along this path they can create a large number of secondary electrons by inelastic scattering. Consequently a large photon penetration depth may be expected to create large numbers of secondary electrons. In contrast, for the opposite case of large absorption constants μ , the incident photons tend to be absorbed closer to the sample surface. In that case primary electrons can escape the sample and create only a relatively small number of secondary electrons along their path before ejection. The number of primary electrons escaping the sample then can become significant compared with that of escaping secondary electrons. Condition (1) thus does not strictly hold.

In addition, Condition (4) is also not fulfilled in the case of large μ . This may be illustrated by the following consideration. Using the absorption constant for 310 eV, which is an energy that is outside the resonance region (Fig. 3), we find a penetration of light that is $1/\mu = 63.7$ nm. For a grazing incidence, as studied in this work, this corresponds to an absorption depth of 24 nm that is measured normal to the surface. In contrast, at the π -resonance near 285 eV, we find a penetration of $1/\mu = 8.6$ nm and a much smaller corresponding absorption

depth of 3 nm below the surface. This latter value is very close to the average escape depth of secondary electrons which is $L = 1.95$ nm. Adopting these results gives a relatively large value for the term that underpins Condition (4) with $\mu L/\cos\theta = 0.66$. It is thus clear that Condition (4), that requires $\mu L/\cos\theta \ll 1$, is not reasonable and should not be applied in this case.

The consideration confirms that, at energies near the 1s carbon edge, equation (7c) should be used and not equation (7a). Importantly, the efficiency of creating secondary electrons depends on the path length of the incident photon and is consequently also energy-dependent. Since M decreases with increasing absorption according to the relation $M \simeq 1/\mu$ and since $M = 1/\varepsilon$, a reasonable approximation may be considered in which the energy-dependence of ε is assumed to have the same functional form as the energy-dependence of η . The mean energy ε may then be expressed as a linear function of η according to

$$\varepsilon = a + b\eta, \quad (9)$$

where a and b are scaling parameters with the dimension energy and conveniently expressed in eV. For $a = 0$, a direct proportionality $M \simeq 1/\mu$ occurs and the energy-dependence of ε is strong. By increasing the scaling parameter a , the effect of the energy-dependence of M is reduced and the energy-dependence becomes eventually insignificant, if the overall magnitude of ε is kept the same.

The simulations that have been carried out with this approach, i.e. using equation (7d), give much better agreement with the reflection data, as it can be seen in Fig. 5. The best agreement was achieved with the scaling parameters $a = 100$ eV and $b = 130$ eV and η taken from Fig. 2. The figure shows that in this case simulation and reflectometry are in good agreement across the π -resonance and also at higher energies (Fig. 5, red). A difference between simulation and data occurring at the low-energy shoulder of the resonance peak, which is not understood, may however be acceptable considering the approximate nature of the energy-dependence chosen for ε . A further difference occurs at 288 eV, where the presence of surface adsorbates on the sample may affect electron yield and reflection measurement differently.

We also checked the efficacy of using equation (7b), which assumes proportionality between TEY and absorption constant in conjunction with an energy-dependent ε . This is also shown in Fig. 5 (violet). It is clear that the energy-dependence of ε improves the simulations with respect to the one based on equation (7a). The result is similar to that using equation (7c) with constant ε . This demonstrates that for a reliable calculation of absorption constants from TEY spectra the energy dependence of the efficiency $M = 1/\varepsilon$ to create secondary electrons should explicitly be considered and that the approximation $\mu L/\cos\theta \ll 1$ needs to be relaxed.

4.3. Dependence of M on absorption and polarization

The reflection spectrum recorded with s -geometry, i.e. the electric field vector of the incident light is perpendicular to the

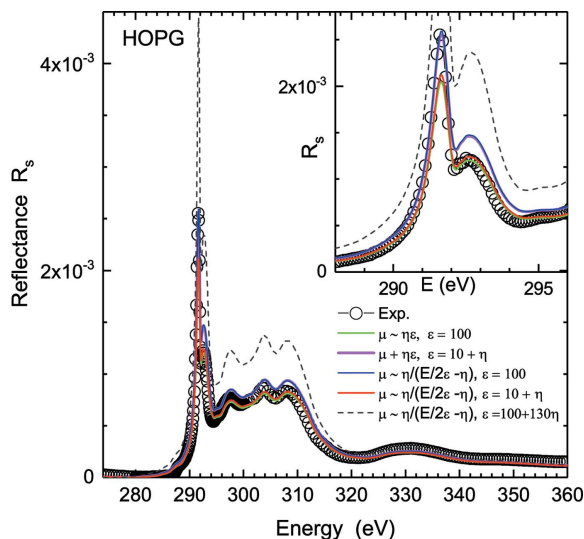


Figure 6 Measured reflectance R_s and simulations for s -geometry. The simulations are discussed in the text. The inset compares data and simulations in more detail at the σ -resonance peak. (The values for ε are given in eV and the dependence of μ on η is indicated.)

scattering plane, differs from that discussed above for p -geometry in several ways. The data are shown in Fig. 6 as open circles and it is apparent that, as expected, the σ -resonance is a pronounced feature. Due to the reduced absorption strength at the σ -resonance the effect of the corrections discussed are not as significant. Nevertheless, as for the π -resonance, simple proportionality between TEY and absorption constant [equation (7a)] does not produce an optimum simulation of the measured spectrum. In particular, the peak at 291 eV is not well reproduced (Fig. 6, green curve).

Applying equation (7c) instead, agreement with the peak height can be obtained, however, incurring a slight overestimation of the second peak at 292.5 eV (blue). The introduction of an energy dependence of ε using a form according to equation (9) does not improve the situation. Fig. 6 shows that best agreement is obtained for $\varepsilon = 10 + \eta$ which corresponds to a small energy-dependent contribution of η of less than 1% effect (red and violet curves).

An explanation for the comparably weak deviation in this case from the simple proportionality between TEY and absorption constant may be provided by reduced absorption strength at energies near the σ -resonance. The relatively weak absorption found corresponds to an absorption depth for photons of about 12 nm below the sample surface. This is four times larger than the value discussed above for p -geometry. Thus the creation depth of primary electrons is about 12 nm and consequently much larger than the typical electron escape depth $L = 1.95$ nm. As a result a large number of electron scattering processes can occur and many secondary electrons are created that exceed the number of primary electrons by far. As a consequence, Condition (4) is fulfilled well and the energy dependence of ε can be safely neglected.

The comparison of results obtained with p - and s -geometry can potentially identify a polarization dependence of the efficiency of creating secondary electrons. Indeed, an effect

has been observed. The scaling parameters a , b which produce a good simulation of the p -geometry data are significantly different for the data recorded with s -geometry. This is illustrated in Fig. 6 with the best result for p -geometry as a black dashed curve, and *vice versa* in Fig. 5. It is clear that for s -geometry the electron creation energy ε needs to be less than for p -geometry. Whereas for p -geometry values of the order of $\varepsilon = (100 + 130\eta)$ eV give reasonable results, for s -geometry ε can only be chosen sensibly between $\varepsilon = (10 + 1\eta)$ eV and $\varepsilon = (100 + 0\eta)$ eV.

This difference in the value for ε , when comparing p - and s -geometry, may be understood by considering the respective orientation of the electric field of the incident light. Semi-classically one may argue that with p -geometry core electrons are often accelerated in a direction that is perpendicular to the sample surface. For the case of strong absorption with many near-surface ionizations of atoms, this can result in the direct ejection of primary electrons from the sample. Consequently few scattering processes occur and the number of secondary electrons is reduced.

In contrast, with s -geometry the electric field vector of the light is parallel to the surface and the predominant direction of motion of the primary electrons remains within the volume of the sample. Thus quite a number of inelastic scattering processes can occur before the electron may escape the sample. This produces more secondary electrons than for the same intensity of linearly polarized light that is incident with p -geometry. In principle the observed and discussed polarization dependence of the electron excitation process of HOPG is directly correlated to the optical birefringence of HOPG (Jansing *et al.*, 2016). In both situations the orientation of the electric field vector plays the dominant role. At π -resonances the parallel alignment to π -bonds leads to strong interaction while at the σ -resonance energy a parallel alignment of the electric field with respect to the σ -bonds leads to strong interactions. Thus the well known optical phenomenon is observed in the above discussion for electron excitation processes.

4.4. Surface roughness

In order to figure out the influence of surface roughness on the simulated reflection spectra, a large number of such calculations were performed using a broad range of roughness values $\zeta = 0$ –12 nm. The roughness ζ reduces the specular reflection and its effects are simulated through the inclusion of the damping factor $\exp(-q^2\zeta^2)$ with $q = 4\pi n/\lambda \cos\alpha$. Here, α is the propagation angle of light in the medium, which is close to θ (Jansing *et al.*, 2016). The damping depends only weakly on the photon wavelength λ and the damping factor is effectively an energy-independent correction. In contrast, the correction factors discussed in this work [equations (7b), (7c) and (7d)] are strongly energy-dependent across the resonance energy. The weak energy-dependence of the damping due to roughness enables a sensitive determination of the mean energy ε of electron creation, since poor choices for that function cannot be compensated by varying the surface roughness.

From the simulations performed in this work a mean surface roughness of $\zeta = 0.7$ nm has been determined for the HOPG sample studied, since this value gives the best agreement for both p - and s -geometry. This roughness value is also consistent with those derived for cleaved HOPG samples by Chang & Bard (1991) and Yang *et al.* (2008).

4.5. Optical constants

The values of the complex refractive index for HOPG, $\tilde{n} = n + ik$, have been deduced from the simulations that gave the best agreement with the reflection data. The associated optical constants are shown in Figs. 7(a) and 7(b) for p - and s -geometry, respectively. Specifically, as described above, the refractive part, $n = 1 - \delta$, has been obtained *via* Kramers–Kronig transformation of the absorption spectrum following the energy-dependent correction of the TEY data using

equation (7d). An uncertainty of less than 8% is estimated for n and k , which we base on variations obtained by analysing other HOPG samples in the same way.

The spectra plotted in Figs. 7(a) and 7(b) as dotted lines represent the optical constants deduced from non-corrected TEY spectra using the conventional proportionality assumption expressed by equation (7a). The underestimation of the peak at the π -resonance can clearly be seen. At the σ -resonance the effect of the correction is much less due to the reduced absorption strength, as discussed above. For comparison the widely used data set for carbon of Henke *et al.* (1993) is shown dashed in Fig. 7. The carbon mass density is 2.25 g cm^{-3} . The data by Henke *et al.* (1993) do not show the π - or σ -resonance peaks and they do not take into account the polarization-dependence of the incident light.

It is instructive to compare the optical constants obtained in this work with those published by us earlier for graphene (Wahab *et al.*, 2018). The two results are in good agreement. The analysis in the earlier paper, which did not consider the efficiency M of secondary electron generation, relied however on an artificial doubling of the mass density. The present analysis has shown that this valid, albeit crude, approach to achieve consistency between absorption and reflection measurements does not have a physics foundation. The correct approach is instead to explicitly include M and its energy-dependence, as we have demonstrated here. The good agreement between the two independent measurements of optical constants for graphene and HOPG, respectively, indicates that, in contrast to many other properties, a two-dimensional graphene sheet does not significantly differ in its soft X-ray optics from the three-dimensional equivalent.

The set of optical constants for HOPG that have been determined in this work and that reconcile best the electron yield and reflection data across the carbon 1s absorption edge are listed in Table S1 of the supporting information.

5. Conclusions

We have presented a new, data-based, approach to determine the optical constants in the soft X-ray range that reconciles simultaneous electron yield and reflection measurements for the same sample. An iterative correction procedure has been developed that takes into account the creation efficiency of secondary electrons. Furthermore an energy-dependence of this efficiency has been introduced. This is important, since the photon absorption depth varies considerably at energies near absorption edges. The correction that has been derived compensates the observed deviation from proportionality of the relationship between absorption and electron yield spectra. The compensation is largest at resonance peaks.

It has been found that the energy-dependence of the efficiency of creating secondary electrons is well represented by the measured electron yield spectrum. The associated mean energy of electron creation for HOPG is across the carbon 1s absorption edge generally of the order of $\varepsilon = 100$ eV. This compares well with the values established by others for gold and copper with photoelectron spectroscopy, which outside

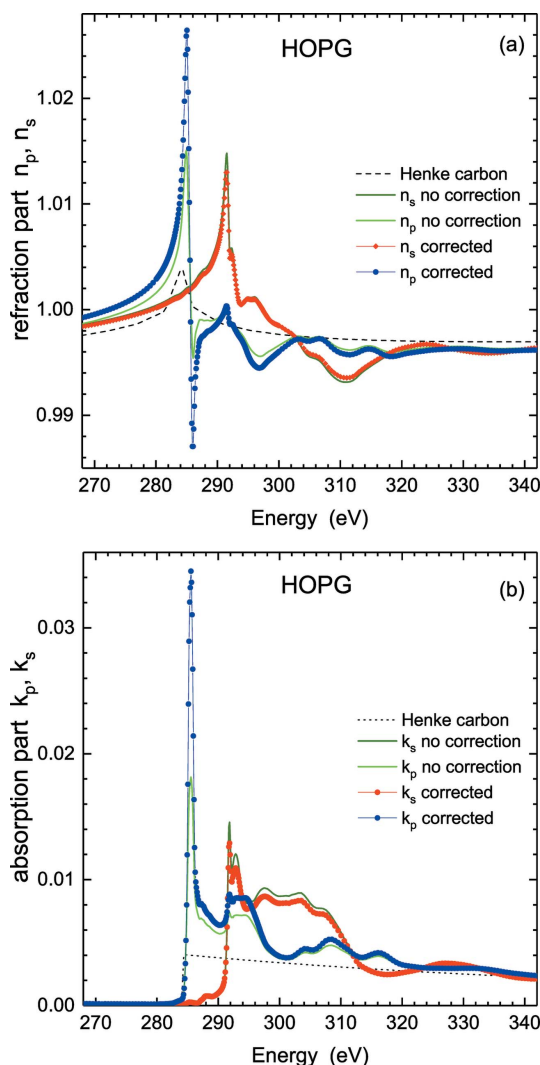


Figure 7
The complex refractive index $\tilde{n} = n + ik$ as best determined in this work for linearly polarized light incident with p -geometry (blue symbols) and s -geometry (red symbols), respectively. (a) The real refractive part $n_{p,s}$. (b) The imaginary absorptive part $k_{p,s}$. For comparison the same is also shown without the correction procedure that has been developed in this work applied (green curves). Reference data for carbon are displayed as the dashed line (from Henke *et al.*, 1993).

resonance regions are $\varepsilon = 64$ eV and $\varepsilon = 26$ eV, respectively. The larger values for HOPG near the carbon 1s absorption resonances indicate that at these energies a reduced number of secondary electrons are created. This is in agreement with the reduction of the absorption depth for photons at the same energies. Consequently quite a number of primary electrons escape the material before they generate secondary electrons via scattering processes.

Importantly, the efficiency of creating secondary electrons has been found to be polarization-dependent. For linearly polarized light incident with *s*-geometry, which strongly excites core electrons at σ -resonance energies, the mean energy of electron creation is significantly lower than for light incident with *p*-geometry, which favourably excites core electrons at the π -resonance. This can be understood semi-classically, since the ejection of primary electrons from the material is favoured with *p*-geometry. In this case the direction of the electric field vector is effectively aligned with the surface normal.

The complete set of optical constants determined in this work is also applicable to other graphitic carbon allotropes such as graphene and it is useful in the description of multilayer systems that contain carbonaceous layers. The new procedure has successfully been demonstrated for HOPG. It can, however, also be used for other materials. The procedure can provide reliable optical constants at energies spanning absorption edges, where typically detailed information on the refractive index is lacking and where such information is most needed in order to perform element-selective spectroscopy.

Funding information

The following funding is acknowledged: Deutscher Akademischer Austauschdienst (grant No. 56270051; grant No. 57215199). Technical and financial support of the Helmholtz-Zentrum Berlin is also acknowledged.

References

Achkar, A. J., Regier, T. Z., Monkman, E. J., Shen, K. M. & Hawthorn, D. G. (2011). *Sci. Rep.* **1**, 182.

- Azzam, R. M. A. & Bashara, N. M. (1987). *Ellipsometry and Polarized Light*. New York, Amsterdam: North Holland.
- Born, M. & Wolf, E. (1959). *Principles of Optics*. Cambridge University Press.
- Chang, H. & Bard, A. J. (1991). *Langmuir*, **7**, 1143–1153.
- Filatova, E. & Sokolov, A. (2018). *J. Synchrotron Rad.* **25**, 232–240.
- Gudat, W. & Kunz, C. (1972). *Phys. Rev. Lett.* **29**, 169–172.
- Henke, B. L., Gullikson, E. & Davis, J. C. (1993). *At. Data Nucl. Data Tables*, **54**, 181–342.
- Henke, B. L., Knauer, J. & Premaratne, K. (1981). *J. Appl. Phys.* **52**, 1509–1520.
- Henneken, H., Scholze, F. & Ulm, G. (1999). *J. Electron Spectrosc. Relat. Phenom.* **101–103**, 1019–1024.
- Henneken, H., Scholze, F. & Ulm, G. (2000). *J. Appl. Phys.* **87**, 257–268.
- Jansing, C., Mertins, H., Gilbert, M., Wahab, H., Timmers, H., Choi, S.-H., Gaupp, A., Krivenkov, M., Varykhalov, A., Rader, O., Legut, D. & Oppeneer, P. M. (2016). *Phys. Rev. B*, **94**, 045422.
- Jiang, H. J. (2011). *Small*, **7**, 2413–2427.
- Krumrey, M., Tegeler, E., Barth, J., Krisch, M., Schäfers, F. & Wolf, R. (1988). *Appl. Opt.* **27**, 4336–4341.
- Mertins, H., Oppeneer, P. M., Valencia, S., Gudat, W., Senf, F. & Bressler, P. R. (2004). *Phys. Rev. B*, **70**, 235106.
- Nakajima, R., Stöhr, J. & Idzerda, Y. U. (1999). *Phys. Rev. B*, **59**, 6421–6429.
- Novoselov, K. S., Fal'ko, V. I., Colombo, L., Gellert, P. R., Schwab, M. G. & Kim, K. (2012). *Nature (London)*, **490**, 192–200.
- Schäfers, F., Mertins, H., Gaupp, A., Gudat, W., Mertin, M., Packe, I., Schmolla, F., Di Fonzo, S., Soullié, G., Jark, W., Walker, R., Le Cann, X., Nyholm, R. & Eriksson, M. (1999). *Appl. Opt.* **38**, 4074–4088.
- Shen, H., Zhang, L. & Liu, M. (2012). *Theranostics*, **2**, 283–294.
- Sohn, K. E., Dimitriou, M. D., Genzer, J., Fischer, D. A., Hawker, C. J. & Kramer, E. J. (2009). *Langmuir*, **25**, 6341–6348.
- Stöhr, J. (1996). *NEXAFS Spectroscopy*. Berlin, Heidelberg: Springer.
- Stöhr, J. & Siegmann, H. C. (2006). *Magnetism, Springer Series in Solid State Sciences*. Berlin, Heidelberg: Springer.
- Wahab, H., Jansing, C., Mertins, H.-Ch., Kim, J. H., Choi, S.-H., Gaupp, A. & Timmers, H. (2018). *Carbon*. In the press.
- Watts, B. (2014). *Opt. Express*, **22**, 23628–23639.
- Weiss, M. R., Follath, R., Sawhney, K. J. S., Senf, F., Bahrtdt, J., Frentrup, W., Gaupp, A., Sasaki, S., Scheer, M., Mertins, H., Abramsohn, D., Schäfers, F., Kuch, W. & Mahler, W. (2001). *Nucl. Instrum. Methods Phys. Res. A*, **467–468**, 449–452.
- Yang, S., Kooij, E. S., Poelsema, B., Lohse, D. & Zandvliet, H. J. W. (2008). *Europhys. Lett.* **81**, 64006.